JNEST EISSN: 2961-8738 ● PISSN: 2961-8916 ● DOI: 10.56741/jnest.v5i03.2599
Article Received 26 August 2026, Revised 18 October 2026

A Comparative Analysis Between PID Controller and Degradation-Aware MPC Controller in PEM Fuel Cell Systems

Gökçe Nur Yildirim*

***Abstract*— Proton Exchange Membrane Fuel Cells (PEMFCs) play a critical role in cyber-physical energy systems and smart buildings. Simultaneous optimization of operational efficiency and long-term stack durability under dynamic load demands requires advanced control strategies. This study presents a comparative analysis between a traditional Proportional-Integral-Derivative (PID) controller and a Degradation-Aware Model Predictive Controller (Da-MPC) under a three-phase dynamic current profile (50A → 70A → 60A) simulated over 300 s. The proposed Da-MPC introduces a Health Index (HI) based reference adaptation law, in which the current setpoint is proportionally attenuated as the catalyst exchange current i0 degrades, thereby embedding durability directly into the closed-loop objective. The controllers are evaluated in terms of transient tracking error (RMSE), settling times, hydrogen consumption, net electrochemical efficiency, and stack degradation states. Results show that the PID controller delivers superior transient tracking with a total RMSE of 2.387 A and settling times of 10.70 s and 6.70 s, but its unconstrained pursuit of the full reference sustains high current density throughout the load cycle and drives a 44.3 % reduction in exchange current (i0 to 0.0557 A). Conversely, Da-MPC deliberately accepts a steady-state tracking offset (total RMSE 7.292 A, settling time > 100 s) in exchange for durability and economy: hydrogen consumption is reduced by 9.76 %, net efficiency is improved by 5.29 % to 242.30 W·s/H_2, and catalyst degradation is limited to 38.0 % (i0 to 0.0620 A), a 14.2 % relative reduction in catalyst loss. Membrane resistance evolved identically for both controllers (Rm=0.00302 Ω), which is consistent with the temperature-driven, current-independent membrane degradation law adopted here.**

***Index Terms*— catalyst degradation, exchange current density, hydrogen consumption, model predictive control, PEM fuel cell, PID control**

I. Introduction

PROTON Exchange Membrane Fuel Cells (PEMFCs) represent a crucial technology for decarbonizing transport, heavy industry, and stationary power networks due to their high-power density and zero localized emissions [1]. However, the widespread commercialization of PEMFCs is severely bottlenecked by two interconnected challenges: the high cost of hydrogen fuel and the degradation-induced short operational lifespan of the fuel cell stack [4]. To address these challenges, researchers have developed advanced modeling and control frameworks to understand, predict, and mitigate the physical aging mechanisms of the stack. An accurate electrochemical and physical representation of the fuel cell is the prerequisite for any effective control strategy. In their seminal work on the Ballard Mark IV PEM fuel cell, researchers established a comprehensive mechanistic model that bridges fundamental thermodynamics and empirical regression [13]. This hybrid approach allows for the analytical calculation of the individual voltage losses—namely activation, internal resistance (ohmic), and concentration overpotentials—under various operating conditions [13]. During real-world dynamic operations, however, the fuel cell stack undergoes severe degradations.

A comprehensive review of prognostics and health management (PHM) frameworks highlights that the polymer membrane and the catalyst-loaded electrodes are the most vulnerable components [4]. The primary aging mechanisms include catalyst active area loss (often modeled as a reduction in the exchange current density, i0, due to platinum dissolution, carbon corrosion, and sintering) and mechanical/chemical membrane thinning leading to hydrogen crossover [4]. While membrane degradation is a highly gradual, predominantly thermally and hygrothermally driven process, electrode degradation is acutely sensitive to the electrical operating point, and in particular to sustained high current density and to the rate of load transitions [4].

To shield the PEMFC stack from the thermal and mechanical stresses of highly fluctuated loads, hybridization with secondary, high-dynamic energy storage systems (ESS)—such as lithium-ion batteries and supercapacitors—is widely implemented. In fuel cell/battery hybrid construction vehicles, multiobjective predictive energy management has been used to distribute power flows so that the PEMFC acts as the steady primary provider while the battery buffers high-frequency transient load spikes, with system models that explicitly include a lifetime component alongside the economic one [2]. Similarly, for heavy-duty applications such as hybrid mining trucks, a nested global optimization search algorithm can simultaneously size the fuel cell/battery components and optimize the energy management strategy (EMS) [9]. Integrating degradation models of both the PEMFC and the Li-ion battery into the EMS has shown to yield nearly a 10 % reduction in the lifecycle cost per ton of mined material [9].

In agricultural tractors, where heavy plowing tasks induce highly dynamic load fluctuations, advanced control models integrate online dynamic response capability [7]. Rather than relying on static constraints, these strategies dynamically update the power boundaries of the fuel cell to prevent reactant starvation while tracking the load [7]. In public transport, triple-source hybrid configurations (PEMFC, battery, and supercapacitor) are utilized in

G. N. Yıldırım (Corresponding author) is with the Department of Mechanical Engineering, Başkent University, 06790 Ankara, Turkey. (e-mail: gokcenur1320@gmail.com).

© 2026 IISTR

modern tramways [5]. To resolve the intrinsic slow response of the fuel cell, a dynamic penalty master-slave control strategy utilizes an equivalent hydrogen consumption minimization strategy (ECMS), with parameters tuned online by an EIA-PSO algorithm, to ensure stable electrical bus performance and reduced fuel consumption [5].

Beyond heavy transport, hydrogen and PEMFC technologies are increasingly integrated into stationary and microgrid systems. To manage highly fluctuated load conditions, a robust hydrogen consumption minimization strategy based on the nature-inspired Salp Swarm Algorithm (SSA) has been proposed [14]. Comparative simulations demonstrate that the SSA-based EMS achieves lower fuel consumption and prevents accelerated stack degradation compared to conventional PI controllers, Genetic Algorithms (GA) [12], and frequency-splitting methods [14]. On a macro-scale, multi-carrier energy systems—such as the integrated Electricity, Heat, and Hydrogen Multi-Energy Storage System (EHH-MESS)—leverage coordinated optimization to enhance power grid flexibility and eliminate the curtailment of large-scale renewable wind and solar energy [11]. At the community and remote area level, stand-alone PV-hydrogen-battery hybrid systems use sizing optimization and advanced control logic to maintain the battery state of charge (SOC) and manage hydrogen reserves [15]. Hierarchical energy management strategies utilizing a two-layer control framework—a local device layer and a system-wide ECMS layer—have been validated through hardware-in-the-loop simulations, ensuring high system longevity and grid stability [8]. In multistack configurations subject to random dynamic loads, deterioration-aware energy management has been shown to extend system lifetime by distributing the load across stacks according to their accumulated damage [3].

Furthermore, optimizing the auxiliary subsystems of the hydrogen economy is vital. For instance, dynamic two-dimensional mathematical modeling of hydrogen storage in metal hydride beds has shown that the strategic placement of concentric cooling systems and active cooling fluid regulation can reduce hydrogen charging times by approximately 60 % [6]. In gas-cooled nuclear reactor systems, advanced spiking neural networks (SNNs)—biologically inspired networks communicating via discrete electrical pulses—are utilized to model and optimize high-temperature hydrogen production without relying on complex, computationally expensive experimental setups [10].

While system-level EMS coordinates power distribution, local-level controllers must regulate the internal parameters of the PEMFC stack. Model Predictive Control (MPC) has emerged as a premier tool due to its native ability to handle multi-variable interactions, state-space constraints, and physical limitations [1]. Experimental demonstrations of various MPC formulations, including explicit and nonlinear MPC (exNMPC), confirm their capability to minimize fuel consumption and prevent reactant starvation while drastically reducing online computational requirements by pre-solving optimal control laws [1]. However, a major gap persists in the literature regarding the treatment of electrode degradation as an endogenous state within the closed loop rather than as an exogenous disturbance, and regarding the quantitative evaluation of the resulting durability-economy-transient response trade-off under dynamic load variation.

Several studies have begun to incorporate durability into the control objective. Lifetime constraints have been embedded in the MPC cost function for PEMFC hybrid power systems by penalizing power slope and stack temperature within the prediction horizon [16]. Nonlinear MPC with a distributed-parameter observer has been used to maximize the active catalytic surface area at the cathode catalyst layer and avoid local starvation [17]. Degradation identification under dynamic load has been formalized as a prognostics problem, enabling the remaining useful life to inform operating decisions [18], and comprehensive reviews have catalogued the failure mechanisms and mitigation measures available at the system level [19]. Health-conscious formulations have further been applied to hybrid ship propulsion [20] and to long-haul fuel cell electric trucks [21], in both cases treating degradation as an explicit optimization target rather than a consequence. These approaches share a common structure: degradation enters either as a constraint or as an additional cost term, while the reference itself remains fixed. The present work differs in that the setpoint is made a function of the measured health state, so that the controller reduces its own demand as the catalyst ages.

The present study addresses this gap through three specific contributions:

- The catalyst and membrane degradation dynamics are embedded directly into the prediction model of the controller, so that the influence of the current setpoint on future catalyst health is visible within the prediction horizon.
- A Health Index based reference adaptation law is proposed, which continuously attenuates the current setpoint in proportion to the measured loss of exchange current, converting durability from a passive outcome into an active closed-loop objective.
- The resulting durability-economy-transient response trade-off is quantified against a finely tuned PID baseline across a three-phase dynamic load profile, providing numerical design guidance for practitioners.

II. PEMFC Modeling and Degradation Formulation

A. Electrochemical Voltage Model

To evaluate controller performance, a control-oriented mathematical model of a 72-cell PEMFC is established. The terminal cell voltage (V_{cell}) is calculated by subtracting polarization losses from the thermodynamic Nernst potential:

$$V_{cell} = E_{Nernst} - V_{act} - V_{ohm} - V_{conc} \quad (1)$$

where V_{act}, V_{ohm}, and V_{conc} represent the activation, ohmic, and concentration polarization losses, respectively [4]. The reversible open-circuit potential is obtained from the Nernst equation, in which the partial pressures of the

reactant gases and the operating temperature determine the thermodynamic ceiling of the cell [13]:

$$E_{Nernst} = E_0 + \left(\frac{RT}{2F}\right)\cdot \ln\left(pH_2.\frac{pO_2^{\frac{1}{2}}}{pH_2O}\right) \quad (2)$$

The activation polarization at the cathode is modeled using the Tafel approximation of the Butler-Volmer relation. This term is the principal coupling point between control action and stack health, because it depends explicitly on the exchange current i0, which in turn reflects the electrochemically active surface area of the platinum catalyst:

$$V_{act} = \left(\frac{RT}{\alpha F}\right)\cdot ln\left(\frac{i}{i_0(t)}\right) \quad (3)$$

The ohmic loss is dominated by proton migration resistance through the membrane, modeled via the membrane resistance $R_m(t)$ [4]:

$$V_{ohm} = i\cdot R_m(t) \quad (4)$$

The concentration loss captures mass-transport limitation as the operating current approaches the limiting current i_{lim}:

$$V_{conc} = -B\cdot ln\left(1 - \frac{i}{i_{lim}}\right) \quad (5)$$

The negative sign is required because $ln\left(1 - \frac{i}{i_{lim}}\right)$ is itself negative for $0 < i < i_{lim}$. Without it, the concentration term would add to rather than subtract from the cell voltage in Equation (1). The total stack voltage and the delivered electrical power are then obtained by summation over the N_c cells of the stack:

$$V_{stack} = N_c\cdot V_{cell}, \quad P_{stack} = V_{stack}\cdot i \quad (6)$$

B. Degradation Dynamics

During fuel cell operation, sustained high electrode potentials and elevated current density cause platinum dissolution and carbon support corrosion, leading to a permanent decrease in the exchange current i0 [4]. This mechanism is represented here by a first-order multiplicative decay law driven by the square of the operating current and accelerated by temperature through an Arrhenius-type factor:

$$\frac{di_0}{dt} = -k_1\cdot i^2\cdot i_0\cdot \exp\left(\frac{T}{T_{ref}}\right) \quad (7)$$

The multiplicative structure of Equation (7) guarantees that i0 remains strictly positive for all admissible trajectories, since the decay rate vanishes as i0 approaches zero. Integrating Equation (7) yields the closed form:

$$i_0(t) = i_0(0)\cdot \exp\left(-k_1\cdot exp\left(\frac{T}{T_{ref}}\right)\cdot \int i^2 dt\right) \quad (8)$$

This shows that the accumulated squared current, rather than the instantaneous current, is the physical driver of catalyst loss. This observation directly motivates the control law proposed in Section III.

Chemical degradation and hygrothermal stress cause thinning and creep of the membrane, represented by a monotonic increase in Rm over long-term operation [4]. In contrast to the catalyst mechanism, membrane aging in the present formulation is driven by the thermal operating point alone and is independent of the current setpoint:

$$\frac{dR_m}{dt} = k_2\cdot \exp\left(\frac{T}{T_{ref}}\right) \quad (9)$$

This structural distinction between Equations (7) and (9) is important for interpreting the results of Section IV: only the catalyst state is controllable through the current setpoint, whereas the membrane state is not influenced by the choice of controller under isothermal operation.

C. Control-Oriented State-Space Model

For controller synthesis, the plant is represented by the state vector:

$$x = [i \;\; i_0 \;\; R_m]^T \quad (10)$$

with the normalized hydrogen inlet flow u as the manipulated variable. The electrical subsystem is approximated by a first-order actuator model, so that the complete nonlinear plant is written as:

$$\frac{di}{dt} = -0.1\cdot i + 0.5\cdot u, \quad \frac{di_0}{dt} as\ in\ (7),\ \frac{dR_m}{dt} as\ in\ (9) \quad (11)$$

Linearizing Equations (7) and (11) about the nominal operating point i_{lin} yields the continuous-time system matrix used inside the predictive controller. The off-diagonal entry A(2,1) is retained deliberately, since it encodes the sensitivity of future catalyst health to the present current level and is precisely the term that makes degradation visible to the optimizer:

$$A(2,1) = -2\cdot k_1\cdot i_{lin}\cdot i_{0,nom}\cdot \exp\left(\frac{T}{T_{ref}}\right),$$

$$A(2,2) = -k_1\cdot i_{lin}^2\cdot \exp\left(\frac{T}{T_{ref}}\right) \quad (12)$$

The complete linearized system matrix therefore takes the lower-triangular form:

$$A = [-0.1, 0, 0; A(2,1), A(2,2), 0; 0, 0, -k_2],$$

$$B = [0.5; 0; 0] \quad (13)$$

In which the sole coupling from the electrical to the electrochemical subsystem is the entry A(2,1).

The full state vector is taken as measurable, C=I3, which renders the pair (A, C) observable and permits the internal state estimator to reconstruct both degradation states. In practice, i0 is inferred from electrochemical impedance spectroscopy or periodic polarization-curve analysis, and Rm from the high-frequency resistance measurement available on commercial test stations; the assumption of full state measurement therefore requires diagnostic instrumentation beyond a standard current sensor. The continuous model is discretized at the sampling period Ts by zero-order hold before being embedded in the predictive controller.

III. Controller Design And Simulation Setup

A. Degradation-Aware MPC with Health Index Reference Adaptation

The predictive controller minimizes a finite-horizon quadratic cost over the prediction horizon Np, penalizing the tracking error of the regulated output, the magnitude of the manipulated variable, and its rate of change:

$$J = \sum[w_y \cdot \big(y(k+j) - r^*(k+j)\big)^2 + w_u \cdot u(k+j)^2 + w\Delta u \cdot \Delta u(k+j)^2] \quad (14)$$

subject to the discretized dynamics of Section II-C and to the actuator saturation constraint $0 \le u \le 100$. Only the current channel is assigned a nonzero output weight; the two degradation states are included in the output vector solely to preserve observability and are not tracked directly.

The distinguishing feature of the proposed Da-MPC is the reference signal r*(k) itself. A Health Index is defined as the instantaneous ratio of exchange current to its nominal value, providing a normalized and directly measurable indicator of catalyst condition:

$$HI(t) = \frac{i_0(t)}{i_{0,nom}} \in [0,1] \quad (15)$$

The Health Index is dimensionless by construction, with HI = 1 denoting a pristine catalyst layer and HI→ 0 denoting complete loss of electrochemically active surface area.

The commanded current setpoint is then continuously attenuated in proportion to the loss of catalyst health, subject to a floor α_h that guarantees a minimum level of service even under severe degradation:

$$r^*(t) = r(t) \cdot [\alpha_h + (1 - \alpha_h) \cdot HI(t)] \quad (16)$$

With the adopted value $\alpha_h = 0.7$, a fully healthy stack (HI=1) is commanded to the unmodified reference, a stack that has lost 20 % of its catalyst activity is commanded to 94 % of the reference, and a stack that has lost 40 % is commanded to 88 %. The mechanism is therefore self-protective: because the degradation rate in Equation (7) scales with i2, reducing the commanded current attenuates the very driver of further catalyst loss, establishing a negative feedback loop on stack aging that is entirely absent from a conventional tracking controller.

B. PID Baseline

The benchmark is a finely tuned PID controller, which represents the industrial standard for fast dynamic response and which tracks the unmodified reference r(t) at all times, irrespective of stack condition:

$$u(t) = K_p \cdot e(t) + K_i \cdot \int e(\tau)d\tau + K_d \cdot \frac{de(t)}{dt},$$
$$e(t) = r(t) - i(t) \quad (17)$$

The integral channel is protected by conditional-integration anti-windup, so that accumulation is suspended whenever the computed command violates the actuator limits. Both controllers operate on the same nonlinear plant, share the same sampling period, and are subject to the same actuator saturation bounds, ensuring that the comparison isolates the effect of the control law itself.

C. Simulation Scenario and Parameters

To test the controllers under representative transient conditions, a three-phase dynamic load profile was simulated over a total duration of 300 s with a sampling period of 0.1 s:

- Phase 1 (0 to 100 s): A steady-state operating phase at a reference current of 50 A, establishing baseline behavior under constant load.
- Phase 2 (100 to 200 s): An abrupt step-up transient to 70 A to evaluate response to sudden high-load demand and the associated acceleration of catalyst degradation.
- Phase 3 (200 to 300 s): A step-down transient to 60 A to assess recovery behavior after the stack has already accumulated measurable damage.

The complete set of physical, degradation, and controller parameters is summarized in Table I. The catalyst degradation coefficient k1 is scaled by a factor of two relative to its nominal physical estimate so that the aging trend becomes observable within the 300 s simulation window; this scaling affects the magnitude of the reported degradation but not the qualitative ordering of the controllers. All simulations were implemented in MATLAB R2022b using the Model Predictive Control Toolbox, with the nonlinear plant integrated by the forward Euler method at the stated sampling period.

TABLE I. Physical, degradation, and controller parameters of the 72-cell PEMFC stack model

Symbol	Description	Value	Unit
N_c	Number of cells in stack	72	-
T	Stack operating temperature	353	K
pH_2	Anode hydrogen partial pressure	1.5	atm
pO_2	Cathode oxygen partial pressure	0.5	atm
E_0	Standard reversible potential	1.229	V
α	Charge transfer coefficient	0.5	-
B	Concentration loss coefficient	0.05	V
i_{lim}	Limiting current	150	A
$i_{0,\,nom}$	Nominal exchange current	0.10	A
$R_{m,\,nom}$	Nominal membrane resistance	0.002	Ω
k_1	Catalyst degradation coefficient	$2x10^{-7}$	$A^{-2}s^{-1}$
k_2	Membrane degradation coefficient	$1x10^{-6}$	$\Omega\ s^{-1}$
T_s	Sampling period	0.1	s
N_p	Prediction horizon	20	steps
N_u	Control horizon	4	steps
w_y	Output tracking weight	1.0	-
w_u	Manipulated variable weight	0.1	-
$w\Delta u$	MV rate weight	0.2	-
α_h	Health adaptation floor	0.7	-
$K_p/K_i/K_d$	PID gains	0.8/0.05/0.01	-

IV. Results and Comparative Analysis

The quantitative results of the comparative study are summarized in Table II. The data reveal a fundamental trade-off between dynamic tracking speed and stack lifetime. The PID controller achieves superior transient speed with a total combined RMSE of 2.387 A and rapid settling times of 10.70 s (50 → 70 A) and 6.70 s (70 → 60 A). However, this aggressive current tracking sustains the stack at high current density for the longest continuous interval of the cycle, causing the exchange current i0 to degrade by 44.3 % (falling to a final value of 0.0557 A). In contrast, the Da-MPC controller attenuates the commanded setpoint through the Health Index law of Equation (16), which leads to slow settling times (> 100 s) and a larger total tracking RMSE of 7.292 A. Nevertheless, the benefits in terms of efficiency and durability are substantial. Da-MPC reduces total normalized hydrogen consumption by 9.76 % (3223.2 vs. 3572.0) and increases

net electrochemical efficiency to 242.30 W·s/H_2. Most importantly, Da-MPC limits the i0 catalyst degradation to 38.0 % (final value of 0.0620 A), preserving the active catalyst layer. Membrane resistance (Rm) followed an identical trajectory for both controllers, rising from 0.002 Ω to 0.00302 Ω, confirming that current-setpoint manipulation preserves the cathode catalyst layer but leaves membrane aging unaffected.

TABLE II. COMPARATIVE PERFORMANCE OF DA-MPC AND PID ACROSS THE THREE-PHASE LOAD PROFILE

Performance Metric	Da-MPC	PID
Transient Tracking		
RMSE Phase 1 (ref=50 A) [A]	1.708	3.162
RMSE Phase 2 (ref=70 A) [A]	7.520	2.386
RMSE Phase 3 (ref=60 A) [A]	10.001	1.186
Total Combined RMSE [A]	7.292	2.387
Response Speed		
Settling Time 50 → 70 A [s]	> 100	10.70
Settling Time 70 → 60 A [s]	> 100	6.70
Fuel & Power Economy		
Total Normalized H2 Consumption [-]	3223.2	3572.0
Average Power Output [W]	2604.2	2740.8
Net Electrochemical Efficiency [W·s/H_2]	242.30	230.12
Stack Lifetime & Aging		
Final Exchange Current i_0 [A]	0.0620	0.0557
i_0 Catalyst Degradation [%]	38.0	44.3
Final Membrane Resistance (R_m) [Ω]	0.00302	0.00302

A. Transient Tracking Performance

Fig. 1 presents the current tracking response and the corresponding hydrogen flow commands. During Phase 1 the Da-MPC attains the reference rapidly and with a low error of 1.708 A, outperforming the PID controller, whose error of 3.162 A originates from the slow charging of its integral channel from a zero initial condition. From Phase 2 onward the ordering reverses. The PID controller reaches the elevated 70 A setpoint within 10.70 s and the subsequent 60 A setpoint within 6.70 s, achieving phase-wise errors of 2.386 A and 1.186 A respectively. The Da-MPC, by contrast, never re-enters the two percent settling band of the unmodified reference, because Equation (16) has by then displaced its effective setpoint below the commanded value. The resulting Phase 2 and Phase 3 errors of 7.520 A and 10.001 A, and the total combined RMSE of 7.292 A, must therefore be read not as a failure of regulation but as the deliberate and quantified price of the durability objective.

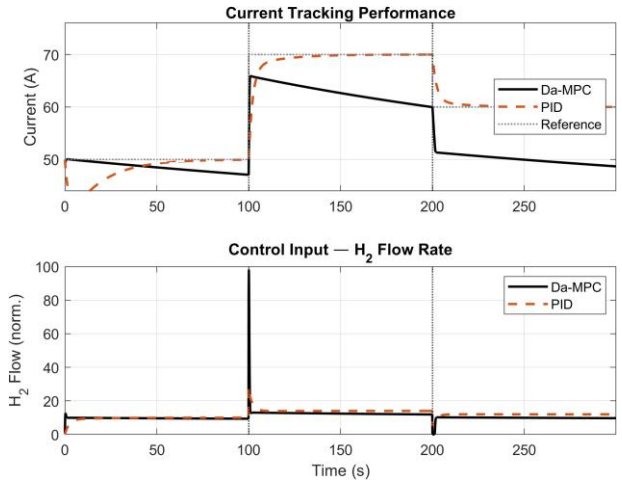

Fig. 1. Current tracking response and the corresponding hydrogen flow commands

B. Voltage and Power Behavior

Fig. 2 decomposes the stack voltage into its constituent polarization losses. The activation overpotential dominates throughout, confirming that the catalyst state is the principal determinant of stack performance under the tested conditions, while the ohmic contribution grows steadily as Rm increases and the concentration term remains small and nearly constant.

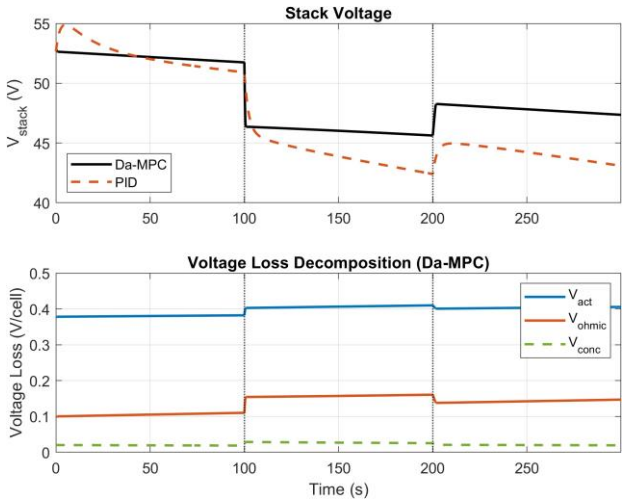

Fig. 2. Stack voltage decomposed into its constituent polarization losses

Fig. 3 shows the delivered stack power. The Da-MPC sustains an average output of 2604.2 W against 2740.8 W for the PID controller, a deficit of 4.98 %. The deficit should be read against the 9.76 % reduction in hydrogen consumption reported in Section IV-C: the Da-MPC gives up proportionally less power than it saves in fuel, which is precisely why its net efficiency is the higher of the two. Crucially, the Da-MPC power trajectory declines gradually within each phase, which is the direct visible signature of the Health Index attenuation acting on the setpoint, whereas the PID trajectory holds its level and declines only through the passive loss of catalyst activity.

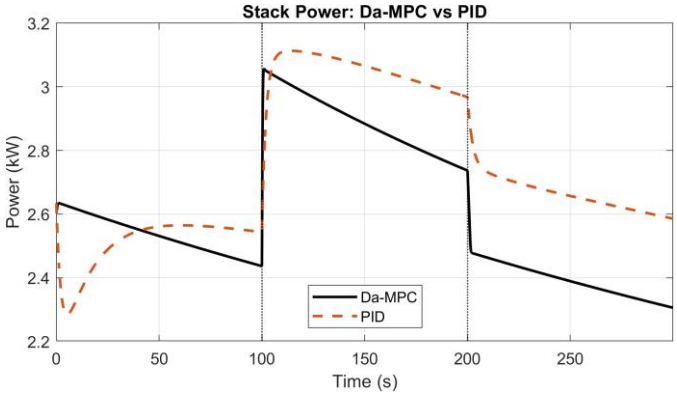

Fig. 3. Delivered stack power

C. Degradation and Fuel Economy

Fig. 4 traces the evolution of both degradation states and constitutes the central result of this study. The exchange current retained under Da-MPC at the end of the cycle is 0.0620 A against 0.0557 A under PID, corresponding to catalyst losses of 38.0 % and 44.3 % respectively. This represents an 11.3 % improvement in retained catalyst activity, or equivalently a 14.2 % relative reduction in catalyst degradation, achieved purely through the choice of

control law and without any change to the physical hardware. The two trajectories separate progressively from approximately 120 s onward, precisely as the accumulated damage becomes large enough for the Health Index to exert a meaningful influence on the commanded setpoint.

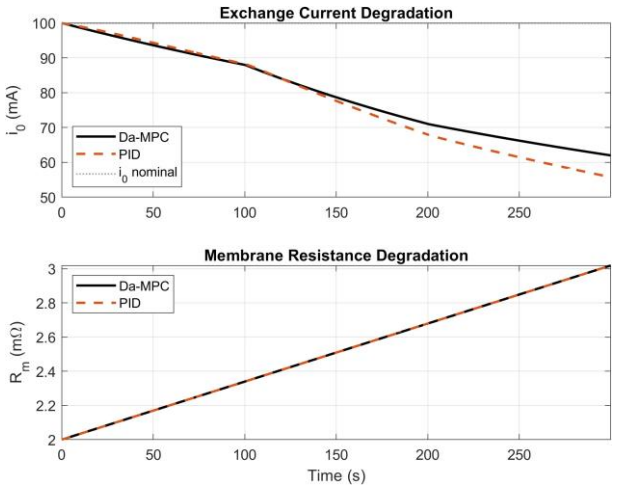

Fig. 4. Evolution of the catalyst exchange current and membrane resistance

The membrane resistance evolves identically for both controllers, rising from 0.002 Ω to 0.00302 Ω. This is the expected consequence of the model structure rather than an absence of aging: as established in Equation (9), the membrane degradation rate depends solely on the thermal operating point, which is held constant in this study, and is therefore structurally insensitive to the current setpoint. It follows that short-horizon control action of the type examined here can protect the cathode catalyst layer but cannot mitigate membrane aging; the latter requires thermal or humidity management as an additional control channel.

Fig. 5 compares cumulative hydrogen consumption. The Da-MPC consumes 3223.2 normalized units against 3572.0 for the PID controller, a reduction of 9.76 %. Combining fuel consumption with delivered power yields a net electrochemical efficiency of 242.30 W·s/H_2 for the Da-MPC against 230.12 W·s/H_2 for the PID controller, an improvement of 5.29 %. The Da-MPC therefore converts each unit of hydrogen into more useful work, even though it delivers less total power, because it operates the stack at a point of lower activation and ohmic loss.

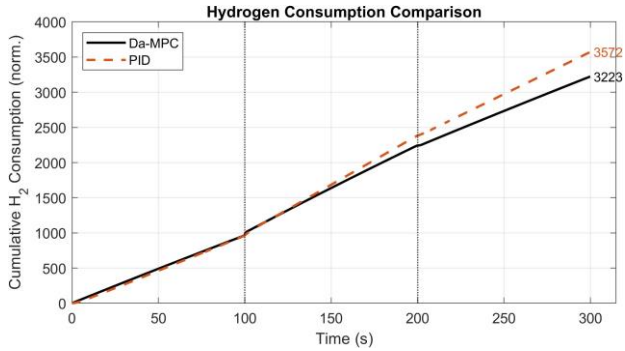

Fig. 5. Cumulative hydrogen consumption comparison

V. Discussion

The results illustrate a durability-economy-transient response trilemma that is intrinsic to PEMFC control design. Because the catalyst degradation rate in Equation (7) scales with the square of the operating current, any controller that pursues an elevated current reference without regard to stack condition necessarily accumulates damage at an accelerated rate. The PID controller does exactly this: its tight tracking of the 70 A demand throughout Phase 2 maintains the stack at the highest current level of the entire cycle for the longest continuous period, and the 44.3 % catalyst loss is the direct arithmetic consequence.

The Da-MPC breaks this coupling by making the reference itself a function of the measured health state. The mechanism is deliberately simple, requiring only the ratio in Equation (15) and a single tuning parameter α_h, which makes it straightforward to implement on embedded hardware alongside an existing predictive controller. The parameter α_h admits a direct engineering interpretation as the guaranteed floor of delivered service under worst-case degradation, and can therefore be negotiated against application requirements rather than tuned blindly.

The principal practical limitation is the transient penalty. A settling time exceeding 100 s is unacceptable for applications requiring fast load following, and this bottleneck must be addressed at the system level rather than within the fuel cell controller. The established remedy is hybridization: pairing the stack with a battery or supercapacitor allows the fast component to absorb the transient while the fuel cell tracks the slow, health-adapted reference [2, 5, 9]. Under such an architecture the tracking deficit reported here is transferred to the storage element and the durability benefit is retained without loss of dynamic performance.

Four limitations of the present study should be acknowledged. First, the degradation laws adopted in Equations (7) and (9) are phenomenological and are calibrated for qualitative rather than quantitative fidelity; validation against accelerated stress test data is required before the reported percentages can be treated as absolute predictions. Second, the model does not resolve reactant partial pressures or local concentration gradients, so mechanisms such as localized oxygen starvation, which the literature identifies as a significant contributor to cathode degradation [1, 4], are not captured and the reported benefit may therefore be conservative. Third, the isothermal assumption removes the temperature channel from the optimization, which by construction excludes any possibility of mitigating membrane aging. Fourth, the assumption of full state measurement (C=I3) presumes access to online estimates of i0 and Rm, which in a production system would require impedance-based diagnostics rather than a current sensor alone.

VI. Conclusion

This study proposed and evaluated a Degradation-Aware Model Predictive Controller for a 72-cell PEMFC stack, in which catalyst and membrane degradation dynamics are embedded in the prediction model and the current setpoint is continuously adapted through a Health Index law. Benchmarked against a finely tuned PID controller across a three-phase dynamic load profile, the following

conclusions are drawn:

- Embedding degradation states in the prediction model and adapting the reference through the Health Index reduced catalyst degradation from 44.3 % to 38.0 %, a relative improvement of 14.2 % in retained catalyst activity, obtained without hardware modification.
- Hydrogen consumption was reduced by 9.76 % and net electrochemical efficiency was improved by 5.29 % to 242.30 $W \cdot s/H_2$, demonstrating that durability and fuel economy are complementary rather than competing objectives under this formulation.
- The durability and economy gains were obtained at the cost of transient performance, with total tracking RMSE rising from 2.387 A to 7.292 A and settling times exceeding 100 s, quantifying the trade-off that a system designer must arbitrate.
- Membrane resistance evolved identically under both controllers, confirming that current-setpoint manipulation protects the cathode catalyst layer exclusively and that mitigating membrane aging requires thermal or humidity actuation as an additional control channel.

Future work will pursue three directions: extending the plant model to resolve reactant partial pressures and stack temperature as controlled states, thereby opening the thermal channel to the optimizer and enabling membrane protection; replacing the fixed adaptation floor α_h with a Pareto-optimal schedule derived from multi-objective optimization, so that the durability-tracking compromise can be selected explicitly; and validating the degradation coefficients against accelerated stress test data to place the reported improvements on a quantitative footing.

CONFLICT OF INTEREST

The author declares no conflict of interest.

REFERENCES

[1] C. Ziogou, S. Voutetakis, M. C. Georgiadis, and S. Papadopoulou, "Model predictive control (MPC) strategies for PEM fuel cell systems: A comparative experimental demonstration," Chemical Engineering Research and Design, vol. 131, pp. 656–670, Mar. 2018, doi: 10.1016/j.cherd.2018.01.024.

[2] T. Li, H. Liu, H. Wang, and Y. Yao, "Multiobjective optimal predictive energy management for fuel cell/battery hybrid construction vehicles," IEEE Access, vol. 8, pp. 25927–25937, 2020, doi: 10.1109/ACCESS.2020.2969494.

[3] J. Zuo, C. Cadet, Z. Li, C. Bérenguer, and R. Outbib, "A deterioration-aware energy management strategy for the lifetime improvement of a multi-stack fuel cell system subject to a random dynamic load," Reliability Engineering & System Safety, vol. 241, Art. no. 109660, Jan. 2024, doi: 10.1016/j.ress.2023.109660.

[4] M. Jouin, R. Gouriveau, D. Hissel, M.-C. Péra, and N. Zerhouni, "Degradations analysis and aging modeling for health assessment and prognostics of PEMFC," Reliability Engineering & System Safety, vol. 148, pp. 78–95, Mar. 2016, doi: 10.1016/j.ress.2015.12.003.

[5] F. Peng, Y. Zhao, X. Li, Z. Liu, W. Chen, Y. Liu, and D. Zhou, "Development of master-slave energy management strategy based on fuzzy logic hysteresis state machine and differential power processing compensation for a PEMFC-LIB-SC hybrid tramway," Applied Energy, vol. 206, pp. 346–363, Nov. 2017, doi: 10.1016/j.apenergy.2017.08.128.

[6] E. S. Kikkinides, M. C. Georgiadis, and A. K. Stubos, "Dynamic modelling and optimization of hydrogen storage in metal hydride beds," Energy, vol. 31, nos. 12–13, pp. 2428–2446, Oct. 2006, doi: 10.1016/j.energy.2005.11.003.

[7] Y. Li, Y. Wu, M. Liu, L. Xu, and S. Lei, "Energy management strategy for hydrogen fuel cell tractors integrating online dynamic response capability," World Electric Vehicle Journal, vol. 17, no. 3, Art. no. 115, Feb. 2026, doi: 10.3390/wevj17030115.

[8] Y. Han, G. Zhang, Q. Li, Z. You, W. Chen, and H. Liu, "Hierarchical energy management for PV/hydrogen/battery island DC microgrid," International Journal of Hydrogen Energy, vol. 44, no. 11, pp. 5507–5516, Feb. 2019, doi: 10.1016/j.ijhydene.2018.08.135.

[9] Y. Feng and Z. Dong, "Integrated design and control optimization of fuel cell hybrid mining truck with minimized lifecycle cost," Applied Energy, vol. 270, Art. no. 115164, Sep. 2020, doi: 10.1016/j.apenergy.2020.115164.

[10] S. O. Starkov and Y. N. Lavrenkov, "Application of spiking neural networks for modelling the process of high-temperature hydrogen production in systems with gas-cooled reactors," Nuclear Energy and Technology, vol. 5, no. 2, pp. 129–137, Jun. 2019, doi: 10.3897/nucet.5.36474.

[11] Y. Teng, Z. Wang, Y. Li, Q. Ma, Q. Hui, and S. Li, "Multi-energy storage system model based on electricity heat and hydrogen coordinated optimization for power grid flexibility," CSEE Journal of Power and Energy Systems, vol. 5, no. 2, pp. 266–274, Jun. 2019, doi: 10.17775/CSEEJPES.2019.00190.

[12] R. Dufo-López, J. L. Bernal-Agustín, and J. Contreras, "Optimization of control strategies for stand-alone renewable energy systems with hydrogen storage," Renewable Energy, vol. 32, no. 7, pp. 1102–1126, Jun. 2007, doi: 10.1016/j.renene.2006.04.013.

[13] J. C. Amphlett, R. M. Baumert, R. F. Mann, B. A. Peppley, P. R. Roberge, and T. J. Harris, "Performance modeling of the Ballard Mark IV solid polymer electrolyte fuel cell: I. Mechanistic model development," Journal of the Electrochemical Society, vol. 142, no. 1, pp. 1–8, Jan. 1995, doi: 10.1149/1.2043866.

[14] A. Fathy, H. Rezk, and A. M. Nassef, "Robust hydrogen-consumption-minimization strategy based salp swarm algorithm for energy management of fuel cell/supercapacitor/batteries in highly fluctuated load condition," Renewable Energy, vol. 139, pp. 147–160, Aug. 2019, doi: 10.1016/j.renene.2019.02.076.

[15] M. Castañeda, A. Cano, F. Jurado, H. Sánchez, and L. M. Fernández, "Sizing optimization, dynamic modeling and energy management strategies of a stand-alone PV/hydrogen/battery-based hybrid system," International Journal of Hydrogen Energy, vol. 38, no. 10, pp. 3830–3845, Apr. 2013, doi: 10.1016/j.ijhydene.2013.01.080.

[16] H. He, S. Quan, F. Sun, and Y.-X. Wang, "Model predictive control with lifetime constraints based energy management strategy for proton exchange membrane fuel cell hybrid power systems," IEEE Transactions on Industrial Electronics, vol. 67, no. 10, pp. 9012–9023, Oct. 2020, doi: 10.1109/TIE.2020.2977574.

[17] J. Luna, E. Usai, A. Husar, and M. Serra, "Enhancing the efficiency and lifetime of a proton exchange membrane fuel cell using nonlinear model-predictive control with nonlinear observation," IEEE Transactions on Industrial Electronics, vol. 64, no. 8, pp. 6649–6659, Aug. 2017, doi: 10.1109/TIE.2017.2682787.

[18] M. Yue, Z. Li, R. Roche, S. Jemei, and N. Zerhouni, "Degradation identification and prognostics of proton exchange membrane fuel cell under dynamic load," Control Engineering Practice, vol. 118, Art. no. 104959, 2022, doi: 10.1016/j.conengprac.2021.104959.

[19] C. Zhang, Y. Zhang, L. Wang, X. Deng, Y. Liu, and J. Zhang, "A health management review of proton exchange membrane fuel cell for electric vehicles: Failure mechanisms, diagnosis techniques and mitigation measures," Renewable and Sustainable Energy Reviews, vol. 182, Art. no. 113369, 2023, doi: 10.1016/j.rser.2023.113369.

[20] C. Dall'Armi, D. Pivetta, and R. Taccani, "Health-conscious optimization of long-term operation for hybrid PEMFC ship propulsion systems," Energies, vol. 14, no. 13, Art. no. 3813, 2021, doi: 10.3390/en14133813.

[21] A. Ferrara, C. Hametner, and S. Jakubek, "Health-conscious predictive energy management strategy for fuel cell electric trucks," Energy Reports, vol. 12, pp. 5961–5973, 2024, doi: 10.1016/j.egyr.2024.11.055.



Gökçe Nur Yildirim is a Research Assistant in the Department of Mechanical Engineering at Başkent University, Ankara, Türkiye. Her research interests encompass nonlinear dynamical systems, control theory, advanced nonlinear control methodologies, and their applications in engineering systems. Her scholarly interests primarily concern the theoretical analysis, mathematical modeling, and development of control strategies for complex dynamical systems, with particular emphasis on system stability, robustness, and performance optimization. (email: gokcenur1320@gmail.com).